Article ID: 1000-5773(2010)02-0093-09

Perforation of Fully-Clamped Thick Metallic Plates Struck Normally by Conical-Nosed Projectiles*

SUN Wei-Hai, WEN He-Ming

(*CAS Key Laboratory for Mechanical Behavior and Design of Materials, University of Science and Technology of China, Hefei* 230027, *China*)

Abstract: Simple analytical equations are given to predict the perforation of fully-clamped thick metallic plates struck normally by rigid conical-nosed projectiles over a wide range of velocities based on the assumption that the deformation is localized and that the impact energy is dissipated only by penetration. It is further assumed that the mean pressure offered by the target materials to resist the projectiles consists of two parts: a quasi-static part due to the elastic-plastic deformation of the laminate materials and a dynamic part due to penetration velocity. Equations are obtained for the residual velocity and ballistic limit. It transpires that the present model predictions are in good agreement with available experimental data for thick metallic plates struck normally by conical-nosed projectiles.

Key words: conical-nosed projectiles; thick metallic plates; ballistic limit; perforation; residual velocity

CLC number: O385 **Document code**: A

1 Introduction

Ballistic perforation is an exceedingly complex mechanical process that has been examined experimentally for the past two centuries and analytically during the last few decades. In particular, the impact behavior of plates is important for the design of engineering and martial structures. The ballistic limit is commonly used to evaluate the performance of plates against projectiles, which is related with the failure modes depending on geometric characteristics, material properties, and impact velocity. Comprehensive reviews on the research can be found in the reviews by Backman *et al*.[1], Corbett *et al*.[2], and Goldsmith[3].

The perforation of a thick plate is controlled by both the penetration process when the processing zone in front of the projectile nose has not reached the rear free surface and the final perforation process when a failure mechanism is initiated in the target in front of the projectile nose. A final failure mechanism, which could be ductile hole enlargement for sharp nose[4], plugging for blunt projectiles[5] or fragment for high impact velocity and brittle target, will be responsible for the final perforation of a target plate. Woodward[6-7] examined the effect of plate thickness and projectile nose geometry on the failure of targets, and discussed the interrelation of different failure modes. Dikshit *et al*.[8] studied the effects of plate thickness and hardness on ballistic performance, and concluded that for thin plates the plastic flow is unconstrained under plane stress conditions, while for thick plates the plastic flow is constrained under plane strain conditions. Børvik *et al*.[9-10] and Dey[11] carried out a series of experiments and numerical simulations on the perforation of steel plates using different projectile nose

* **Received date**: 2009-03-02; **Revised date**: 2009-06-04

Author Biography: SUN Wei-Hai(1982—), male, doctoral candidate, major in impact dynamics. E-mail: weihai_sun@163.com

Corresponding Author: WEN He-Ming(1965—), male, professor, major in impact dynamics. E-mail: hmwen@ustc.edu.cn

shapes. Hill[12] studied the quasi-static cavity expansion of infinite targets and derived the formula of pressure on the surface of cavity. Forrestal[4,13], Warren[14], Zhou and Wen[15] presented cylindrical cavity expansion models for the penetration and perforation of ductile metal targets with different material constitutive relationships impacted by rigid conical-nosed projectiles. Warren *et al*.[16] performed experiments and simulations of oblique penetration of aluminum targets by ogive-nosed steel projectiles, and constructed a decay function to account for the effect of a finite boundary. Wen[17-18] proposed a target resistance formula with the incident speed and investigated the perforation and penetration of the target under impact by projectiles with different noses. Chen *et al*.[19] studied the perforation of a thick plate by rigid projectiles based on the dynamic cavity expansion model. He *et al*.[20-21] obtained the equations for the depth of penetration and ballistic limit of fibre-reinforced plastic (FRP) laminates by using a resistance pressure formula related with the instantaneous velocity of projectile. Ben-Dor[22] gave a comprehensive review on the recent analytical models of plate penetration dynamics.

In this paper, a theoretical study is presented on the perforation of thick metallic plates struck normally by conical-nosed projectiles. The formulations are based on the assumption that the deformation is localized and that the pressure offered by the target materials to resist the projectiles is no longer a constant as proposed in Ref. [17] and Ref. [18], rather a function of penetration velocity. Equations are obtained for residual velocity and ballistic limit. The theoretical predictions are compared with available experimental data and discussed.

2 Analytical Model

2.1 Assumption about the Resistive Pressure

For thick plates, only local deformation needs to be considered and the global response can be neglected. Along with the increasing plate thickness, the influence of plate material inertia will increase. A dynamic pressure term related with the projectile velocity is introduced into the mean resistive pressure here to take into account for the inertia effect. Based on the study of He *et al*.[21], it is assumed that the mean pressure applied normally to the surface of a projectile by a metallic plate to resist the projectile motion can be decomposed into two parts: one part is the quasi-static resistive pressure ($f\sigma_s$) and the other is the dynamic resistive pressure (σ_d) arising from velocity effects, namely $\sigma_n = f\sigma_s + \sigma_d$. Employing the dynamic pressure term proposed by He *et al*.[21], namely $\sigma_d = \beta(\rho_t\sigma_y)^{1/2}V_n$, the mean resistive pressure for a thick plate perforated by a rigid projectile is

$$\sigma_n = f\sigma_s + \beta(\rho_t\sigma_y)^{1/2}V_n \tag{1}$$

where β is a constant which is determined empirically, ρ_t is the density of the metallic plates, V_n is the velocity normal to the surface of the projectile. There is a difference that the quasi-static resistive pressure is no longer the linear elastic limit in through-thickness compression as proposed in Ref. [21], but the quasi-static resistive pressure (σ_s) of cylindrical cavity expansion with a modification function (f).

Here the quasi-static resistive pressure is discussed firstly. When a conical-nosed rigid projectile penetrates an infinite target of an elastic linear-hardening material at normal incidence, the quasi-static cylindrical cavity expansion analysis yields a general relationship between the normal resistive pressure σ_s on the projectile nose and the yielding stress σ_y following Tresca criterion and incompressibility[12]

$$\sigma_s = \frac{\sigma_y}{2}\left(1 + \ln\frac{2E}{3\sigma_y}\right) + \frac{\pi^2 E_p}{18} \tag{2}$$

where E and E_p are elastic and linear-hardening modulus respectively.

For the perforation of finite thickness plates, because the thickness of materials is limited in the direction of cavity expansion and the plastic flow is not fully constrained[8], the modifications to

account for free surface effects need to be considered in the expression of resistive pressure. Warren *et al*.[16] constructed a modification function to account for free surface effect in the dynamic spherical cavity expansion model, which depended on a distance to the free surface. Based on the methods of Warren *et al*.[16], He[23] obtained a modification function of free surface effect in the dynamic cylindrical cavity expansion model. Here a modification function is constructed to account for the effects of a finite boundary in the quasi-static cylindrical cavity expansion, and modify the resistive pressure of materials. The function expression is

$$f(H,d,\theta)=\begin{cases}\ln\left[1+\dfrac{NH}{d\sin(\theta/2)}\right]\dfrac{\sigma_y}{\sigma_s} & \dfrac{H}{d}<K_1\\ 1 & \dfrac{H}{d}\geqslant K_1\end{cases} \tag{3}$$

where H is the target thickness, d and θ are shank diameter and cone angle of the conical-nosed projectile, and N is a constant which is determined empirically. K_1 is a critical H/d ratio, above which free surface effects can be neglected, i. e. $f=1$. K_1 is derived by setting $f=1$ in Eq. (3), which can be expressed as

$$K_1=\frac{1}{N}\sin\frac{\theta}{2}\left\{\exp\left[\frac{1}{2}\left(1+\ln\frac{2E}{3\sigma_y}\right)+\frac{\pi^2E_p}{18\sigma_y}\right]-1\right\} \tag{4}$$

Combining Eq. (2) and Eq. (3) gives the resistive pressure applied normally to the surface of a conical-nosed projectile in the process of plate perforation, namely

$$\sigma_n=f\sigma_s=\alpha\sigma_y \tag{5}$$

The coefficient α is defined as

$$\alpha=\frac{\sigma_s f(H,d,\theta)}{\sigma_y}=\begin{cases}\ln\left[1+\dfrac{NH}{d\sin(\theta/2)}\right] & \dfrac{H}{d}<K_1\\ \dfrac{1}{2}\left[1+\ln\dfrac{2E}{3\sigma_y}\right]+\dfrac{\pi^2E_p}{18\sigma_y} & \dfrac{H}{d}\geqslant K_1\end{cases} \tag{6}$$

Substituting Eq. (2) and Eq. (5) into Eq. (1) and rearranging yields

$$\sigma_n=f\sigma_s+\beta V_n(\rho_t\sigma_y)^{1/2}=\omega+\xi V_z \tag{7}$$

where $\omega=\alpha\sigma_y$, $\xi=\beta(\rho_t\sigma_y)^{1/2}\sin(\theta/2)$, V_z is the projectile velocity in axial direction.

It has to be mentioned here that the present model assumes hole enlargement dominates in the whole perforation process, and does not address all the actual physical behaviors-bulge, necking, plate cracking, friction, etc., rather, all these effects have been lumped into the resistive pressure.

2.2 Perforation Equations for a Conical-Nosed Projectile

Fig. 1 and Fig. 2 show a conical-nosed projectile perforating metallic targets which can be divided into two cases depending on the ratio of the target thickness (H), to the nose length (L_n), then each case contains three stages. z is instant perforation displacement of the projectile in axial direction, σ_n is the normal pressure on the projectile nose, so the axial resistive forces can be integrated.

2.2.1 Case Ⅰ: $H\leqslant L_n$

Fig. 1 shows that the perforation process can be divided into three stages: $z\leqslant H$, $H<z\leqslant L_n$ and $z>L_n$. The axial resistive forces in these stages can be written as

$$F_z=\begin{cases}\pi z^2\tan^2(\theta/2)\sigma_n & z\leqslant H\\ \pi(2z-H)H\tan^2(\theta/2)\sigma_n & H<z\leqslant L_n\\ \pi\left[L_n^2-(z-H)^2\right]\tan^2(\theta/2)\sigma_n & z>L_n\end{cases} \tag{8}$$

And the equation of motion of the projectile is

$$G\frac{\mathrm{d}V_z}{\mathrm{d}t}=GV_z\frac{\mathrm{d}V_z}{\mathrm{d}z}=-F_z \tag{9}$$

Substituting Eq. (7) and Eq. (8) into Eq. (9), we obtained the following expressions

$$\frac{1}{3}H^3=\frac{G\{(V_s-V_1)-\omega\xi^{-1}\ln[(1+\xi\omega^{-1}V_s)/(1+\xi\omega^{-1}V_1)]\}}{\pi\xi\tan^2(\theta/2)} \tag{10}$$

$$HL_n(L_n-H)=\frac{G\{(V_1-V_2)-\omega\xi^{-1}\ln[(1+\xi\omega^{-1}V_1)/(1+\xi\omega^{-1}V_2)]\}}{\pi\xi\tan^2(\theta/2)} \tag{11}$$

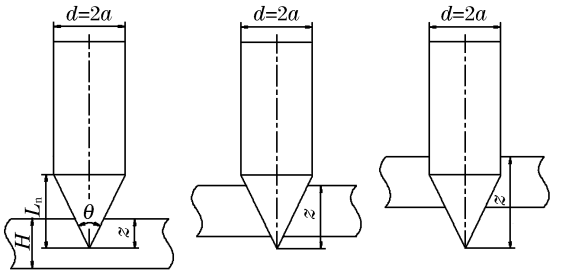
$$H^2(L_n-\frac{1}{3}H)=\frac{G\{(V_2-V_r)-\omega\xi^{-1}\ln[(1+\xi\omega^{-1}V_2)/(1+\xi\omega^{-1}V_r)]\}}{\pi\xi\tan^2(\theta/2)} \tag{12}$$

where V_1, V_2 and V_r are the projectile velocities at the end of the first, second and third stages, respectively; V_s is the incident velocity of the projectile. Combining Eq. (10)～Eq. (12) and eliminating V_1, V_2 yields an equation for the residual velocity, namely

$$V_r=V_s-\omega\xi^{-1}\ln[(1+\xi\omega^{-1}V_s)/(1+\xi\omega^{-1}V_r)]-\pi\xi Hd^2/4G \tag{13}$$

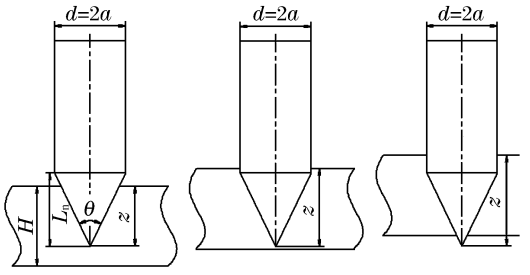
Then set $V_r=0$ in the above equation, one obtains an expression for the ballistic limit velocity

$$V_c=\omega\xi^{-1}\ln(1+\xi\omega^{-1}V_c)+\pi\xi Hd^2/4G \tag{14}$$



(a) $z\leqslant H$ (b) $H<z\leqslant L_n$ (c) $z>L_n$

Fig. 1 Schematic diagram of a conical-nosed projectile perforating a metallic plate with $H\leqslant L_n$



(a) $z\leqslant L_n$ (b) $L_n<z\leqslant H$ (c) $H<z\leqslant L_n+H$

Fig. 2 Schematic diagram of a conical-nosed projectile perforating a metallic plate with $H>L_n$

2.2.2 Case Ⅱ: $H>L_n$

Fig. 2 shows that the perforation process can also be divided into three stages: $z\leqslant L_n$, $L_n<z\leqslant H$ and $H<z\leqslant L_n+H$. The axial resistive forces in these stages can be expressed as

$$F_z=\begin{cases}\pi z^2\tan^2(\theta/2)\sigma_n & z\leqslant L_n\\ \pi L_n^2\tan^2(\theta/2)\sigma_n & L_n<z\leqslant H\\ \pi[L_n^2-(z-H)^2]\tan^2(\theta/2)\sigma_n & H<z\leqslant L_n+H\end{cases} \tag{15}$$

Substituting Eq. (7) and Eq. (15) into Eq. (9), thus we have

$$\frac{1}{3}L_n^3=\frac{G\{(V_s-V_1)-\omega\xi^{-1}\ln[(1+\xi\omega^{-1}V_s)/(1+\xi\omega^{-1}V_1)]\}}{\pi\xi\tan^2(\theta/2)} \tag{16}$$

$$L_n^2(H-L_n)=\frac{G\{(V_1-V_2)-\omega\xi^{-1}\ln[(1+\xi\omega^{-1}V_1)/(1+\xi\omega^{-1}V_2)]\}}{\pi\xi\tan^2(\theta/2)} \tag{17}$$

$$\frac{2}{3}L_n^3=\frac{G\{(V_2-V_r)-\omega\xi^{-1}\ln[(1+\xi\omega^{-1}V_2)/(1+\xi\omega^{-1}V_r)]\}}{\pi\xi\tan^2(\theta/2)} \tag{18}$$

where V_1, V_2 and V_r are also the projectile velocities at the end of the first, second and third stages in this case, respectively. Combining Eq. (16)～Eq. (18) and eliminating V_1, V_2 yields an equation for the residual velocity, namely

$$V_r=V_s-\omega\xi^{-1}\ln[(1+\xi\omega^{-1}V_s)/(1+\xi\omega^{-1}V_r)]-\pi\xi Hd^2/4G \tag{19}$$

Then set $V_r=0$ in the equation, the ballistic limit velocity can be formulated as

$$V_c=\omega\xi^{-1}\ln(1+\xi\omega^{-1}V_c)+\pi\xi Hd^2/4G \tag{20}$$

By comparing Eq. (20) with Eq. (14), it is interesting to note that the equations for residual velocity and ballistic limit velocity are same for above two cases although the perforation processed are different.

3 Results and Discussion

In this section, analytical equations derived in Section 2 are compared with available experimental data and discussed. In the calculation, it is assumed that the projectile remains undeformed; σ_y and E_p are yielding stress and linear-hardening modulus of the plate material respectively. However in some literatures there are yielding stress (σ_y) and ultimate stress (σ_u) of the target material, but no hardening modulus (E_p). In such situation the average yielding stress which is used to solve the above expressions is calculated from $(\sigma_y+\sigma_u)/2$, and the hardening modulus is set to zero.

It should be mentioned that the model proposed in Section 2 is applicable for thick plates. For the perforation of thick plates, generally the global response is neglected and only local deformation is considered. Here a criterion for differentiating a thin plate from a thick target is proposed by comparing the collapse load with the maximum local piercing load. Based on the quasi-static deformation theory of ductile materials proposed by Wen and Jones[24], the maximum transverse displacement W_{om} at the periphery of the projectile-plate interface is determined by the maximum resistive force F_{max} in the perforation process, namely

$$W_{om}=(F_{max}-F_c)/K_m \tag{21}$$

where $K_m=2\pi\sigma_y H/\ln(R/a)$ is the plate membrance stiffness; $F_c=(1/\sqrt{3})\pi\sigma_y H^2[1+(1+\sqrt{3}/2)/\ln(R/a)]$ is the static collapse load of the plate for infinitesimal displacements, when resistive force is larger than this load, the global deflection begins to occur; R and a are outer radius of the clamped metallic plate and shank radius of the projectile respectively.

From Eq. (21), it is known that when $F_{max}>F_c$, there is $W_{om}>0$, the plate is classified to a thin plate, and both its local and global deformations should be taken into account in the perforation by a conical-nosed projectile; when $F_{max}\leqslant F_c$, there is $W_{om}=0$, the plate can be regarded as a thick plate, only its local deformation needs to be considered. In this paper, the perforation of thick plates is discussed. Here K_2 is introduced to satisfy $H/d=K_2$ when $F_{max}=F_c$. Then the criterion can be restated as that when $H/d<K_2$, the plate is a thin plate; when $H/d\geqslant K_2$, there is $W_{om}=0$ and the plate can be regarded as a thick plate. Combining Eq. (6) and the expression $L_n=(d/2)/\tan(\theta/2)$ to solve the equation $W_{om}=0$, K_2 can be calculated. The perforation of fully-clamped thick metallic plates struck by rigid conical-nosed projectiles at ballistic limit, according to the values of K_1 and K_2, can be divided into following situations: (Ⅰ) when $K_1>K_2$, there are two situations, namely, (1) $K_2<H/d\leqslant K_1$, $0<f\leqslant 1$, (2) $H/d>K_1$, $f=1$; (Ⅱ) when $K_1\leqslant K_2$, there is $H/d>K_2$, $f=1$.

In the following, a collection of experimental data for thick plates is compared with the present analytical prediction. These experimental results fall in the category of impacting by non-deformable projectiles. In Eq. (7), β is an empirical constant which needs to be determined. Based on the work in He *et al*.[21], it is assumed that for conical-nosed projectiles β in Eq. (7) is dependent on cone angle and can be written as $\beta=c_1+c_2\sin(\theta/2)$ where c_1, c_2 are evaluated to be 1 and 4 by calibrating against the experimental results for 5083 aluminum plates perforated by a 8.31 mm diameter conical-nosed projectile with $G=25.8$ g, $\theta=31.3°$[13] and a 4.76 mm diameter conical-nosed projectile with $G=2.83$ g, $\theta=45°$[25], respectively. The parameters of the 5083 aluminum plates are $E=70$ GPa, $\rho_t=2\,700$ kg/m^3, and the mechanical properties are $\sigma_y=380$ MPa, $E_p=60$ MPa and $\sigma_y=380$ MPa, $E_p=60$ MPa, respectively. Then the values of K_1 and K_2 are calculated to be $K_1=0.70$, $K_2=0.75$ and $K_1=1.0$, $K_2=0.76$ respectively, so two groups of experimental data all satisfy $f=1$ and conditions of the thick plate theory. Thus

$$\beta=1+4\sin(\theta/2) \tag{22}$$

It can be seen from Fig. 3 and Fig. 4 that the model predictions with $\beta=1+4\sin(\theta/2)$ are in good agreement with the test data for the perforation of 5083 aluminum plates impacted by conical-nosed projectiles.

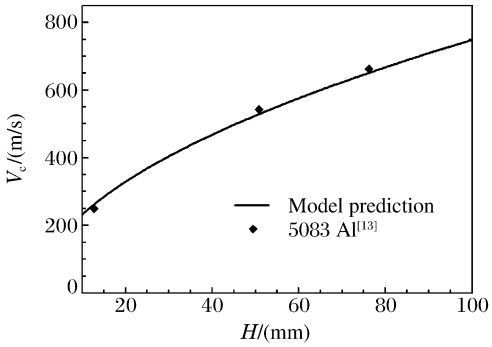


Fig. 3 Comparison of the theoretical predictions with the experimental data[13] for the ballistic limit of 5083 Al plates with three thicknesses struck transversely by 8.31 mm diameter, 25.8 g conical-nosed projectiles

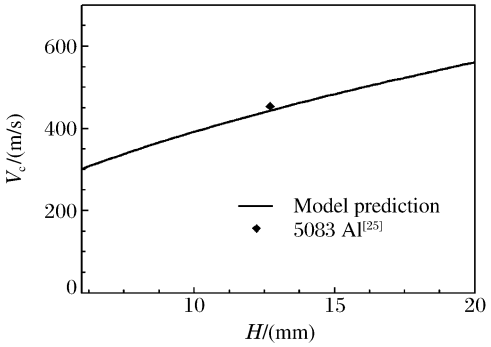


Fig. 4 Comparison of the theoretical prediction with the experimental data[25] for the ballistic limit of 12.7 mm 5083 Al plate struck transversely by a 12.7 mm diameter, 2.83 g conical-nosed projectile

The validity of the thick plate model is verified against more experimental data in the following. Fig. 5 shows comparison between the theoretically predicted ballistic limits and the experimental results for 5083 aluminum plates struck transversely by a 197 g, 33.4° cone angle and 20 mm diameter conical-nosed projectile[10]. The parameters of target are $\rho_t=2\,700$ kg/m^3, $E=70.3$ GPa, $\sigma_y=240$ MPa, $E_p=310$ MPa. Here $\beta=1+4\sin(\theta/2)=2.15$. Then it is obtained that $K_1=0.90$, $K_2=0.72$. Therefore the perforation of 15 mm plate meets $K_2<H/d\leqslant K_1$, $0<f\leqslant 1$ and the perforation of plates with other three thicknesses meets $H/d>K_1$, $f=1$, both can be solved by the thick plate theory. It can be seen that the theoretical predictions of Eq. (14) or Eq. (20) agree well with the experimental data reported by Børvik *et al*.[10] except for the 25 mm plates. A small "kink" in the ballistic limit versus target thickness curve seems to appear at a thickness of about 25 mm. However, this kink seems not to be related to a change in deformation mode with target thickness, but is more likely due to experimental or material variations as reported in Ref. [10]. Here the constant N in Eq. (3) and Eq. (6) is calibrated to 6 according to the experimental data in Ref. [26].

Table 1 shows both the predictions and test data of perforation of thick plates by conical-nosed projectiles. As shown in the table, theoretical analyses show good agreement with the individual published test data of projectiles with different cone angles and thick plates with different thicknesses. The

Table 1 Comparison of ballistic test data and model predictions of thick metallic plates

No.	Projectiles			Plates							$V_{c,exp}$ /(m/s)	$V_{c,calc}$ /(m/s)
	d /(mm)	θ /(°)	G /(g)	Materials	ρ /(kg/m^3)	H /(mm)	E /(GPa)	σ_y /(MPa)	σ_u /(MPa)	E_p /(MPa)		
1[25]	4.76	45	2.83	Mild steel	7 800	4.78	200	450		526	375	363
2[25]	6.35	45	3.03	Mn steel	7 800	6.35	200	455		1 240	603	613
3[25]	4.76	45	2.83	Al	2 700	6.35	70	150		79	225	223
4[25]	6.35	45	3.03	Al	2 700	6.35	70	150		79	293	294
5[4]	10.2	39	78	6061 Al	2 660	25.4	70.3	288	313		235	229
6[27]	7.1	39	25	6061 Al	2 660	25.4	70.3	288	313		315	306

formula for the ballistic limit of thick plates leads to an excellent prediction.

Comparisons are made in Fig. 6～Fig. 8 between the theoretical and measured residual velocities for the perforation of the fully-clamped thick metallic plates struck by conical-nosed projectiles. Fig. 6 shows the results that 5083 aluminum plates with three different thicknesses of 12.7, 50.8 and 76.2 mm is perforated by a 8.31 mm diameter conical-nosed projectile with $G=25.8$ g, $\theta=31.3°$ in Ref. [13], the parameters of target are $\rho_t=2\,700$ kg/m^3, $E=70$ GPa, $\sigma_y=380$ MPa, $E_p=60$ MPa.

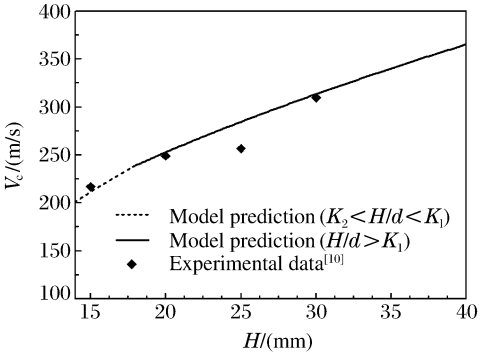


Fig. 5　Comparison of the theoretical predictions with the experimental data from Ref. [10] for the ballistic limits of 5083 Al plates with four thicknesses struck transversely by 20 mm diameter, 197 g conical-nosed projectiles

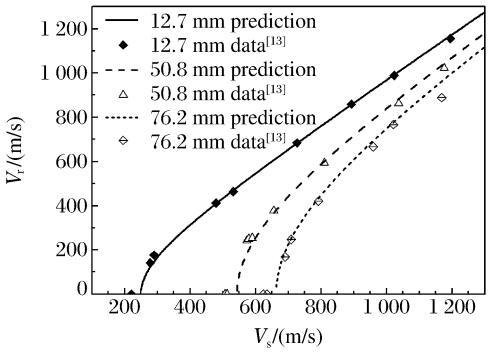


Fig. 6　Comparison of the theoretical predictions with the experimental data from Ref. [13] for the residual velocity of three thickness 5083 Al plates struck transversely by 8.31 mm diameter, 25.8 g conical-nosed projectiles

Fig. 7 shows the results that 5083-H116 aluminum plates with four different thicknesses of 15, 20, 25, and 30 mm is perforated by a 20 mm diameter conical-nosed projectile with $G=197$ g, $\theta=33.4°$ in Ref. [10], the parameters of target are $\rho_t=2\,700$ kg/m^3, $E=70.3$ GPa, $\sigma_y=240$ MPa, $E_p=310$ MPa.

Fig. 8 shows the results that 6061-T6 aluminum plates with thickness of 25.4 mm is perforated by a 7.1 mm diameter conical-nosed projectile with $G=25$ g, $\theta=39°$ in Ref. [27], the parameters of target are $\rho_t=2\,660$ kg/m^3, $E=70.3$ GPa, $\sigma_y=300.5$ MPa, $E_p=0$. As shown in Fig. 6～Fig. 8, the present predicted residual velocities agree well with the experimental data, whereas the predictions of 25 mm plates in Fig. 7 shows some discrepancy from the experimental results. This discrepancy may come from experimental and materials variations in Ref. [10].

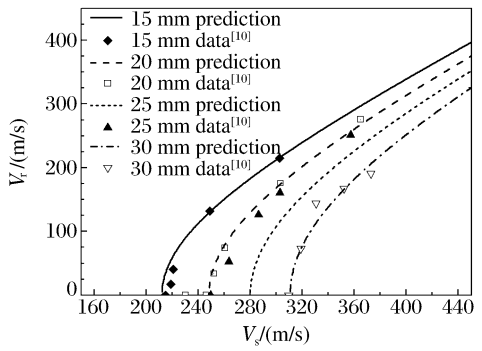


Fig. 7　Comparison of the theoretical predictions with the experimental data from Ref. [10] for the residual velocity of four thickness 5083 Al plates struck transversely by 20 mm diameter, 197 g conical-nosed projectiles

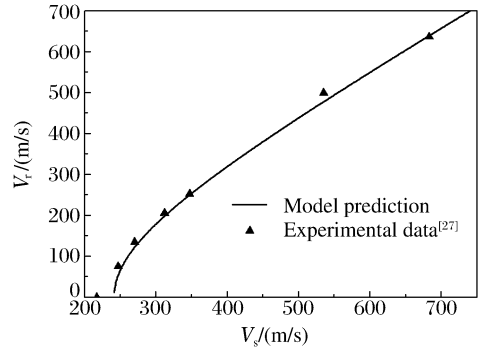


Fig. 8　Comparison of the theoretical predictions with the experimental data from Ref. [10] for the residual velocity of 25.4 mm 6061 Al plate struck transversely by 7.1 mm diameter, 25 g conical-nosed projectiles

4 Conclusions

A theoretical study has been carried out on the perforation of fully-clamped thick metallic plates struck normally by conical-nosed projectiles with different cone angles over a wide range of velocities. The formulations are based on the assumption that the deformation is localized and that the pressure offered by the metallic targets to resist the projectile is velocity dependent which can be divided into two parts: a quasi-static part due to the elastic-plastic deformation of the target materials, and a dynamic part due to penetration velocity. Simple analytical equations have been obtained for the ballistic limit and residual velocity. It transpires that the present theoretical predictions of perforation agree well with available experimental data of different plates struck by conical-nosed projectiles with different cone angles in terms of ballistic limit and residual velocity.

References:

[1] Backman M E, Goldsmith W. The Mechanics of Penetration of Projectiles into Targets [J]. Int J Eng Sci, 1978, 16(1): 1-99.

[2] Corbett G G, Reid S R, Johnson W. Impact Loading of Plates and Shells by Free-Flying Projectiles: A Review [J]. Int J Impact Eng, 1996, 18(2): 141-230.

[3] Goldsmith W. Non-Ideal Projectile Impact on Targets [J]. Int J Impact Eng, 1999, 22(2-3): 95-395.

[4] Forrestal M J, Rosenberg Z, Luk V K, et al. Perforation of Aluminum Plates with Conical-Nosed Rods [J]. J Appl Mech, 1987, 54(1): 230-232.

[5] Børvik T, Langseth M, Hopperstad O S, et al. Ballistic Penetration of Steel Plates [J]. Int J Impact Eng, 1999, 22(9-10): 855-886.

[6] Woodward R L. The Interrelation of Failure Modes Observed in the Penetration of Metallic Targets [J]. Int J Impact Eng, 1984, 2(2): 121-129.

[7] Woodward R L, Cimpoeru S J. A Study of the Perforation of Aluminium Laminate Targets [J]. Int J Impact Eng, 1998, 21(3): 117-131.

[8] Dikshit S N, Kutumbarao V V, Sundararajan G. The Influence of Plate Hardness on the Ballistic Penetration of Thick Steel Plates [J]. Int J Impact Eng, 1995, 16(2): 293-320.

[9] Børvik T, Hopperstad O S, Berstad T, et al. Perforation of 12 mm Thick Steel Plates by 20 mm Diameter Projectiles with Flat, Hemispherical and Conical Noses, Part II: Numerical Simulations [J]. Int J Impact Eng, 2002, 27(1): 37-64.

[10] Børvik T, Clausen A H, Hopperstad O S, et al. Perforation of AA5083-H116 Aluminium Plates with Conical-Nose Steel Projectiles—Experimental Study [J]. Int J Impact Eng, 2004, 30(4): 367-384.

[11] Dey S, Børvik T, Hopperstad O S, et al. The Effect of Target Strength on the Perforation of Steel Plates Using Three Different Projectile Nose Shapes [J]. Int J Impact Eng, 2004, 30(8-9): 1005-1038.

[12] Hill R. The Mathematical Theory of Plasticity [M]. New York: Oxford University Press, 1950: 125-127.

[13] Forrestal M J, Luk V K, Brar N S. Perforation of Aluminum Armor Plates with Conical-Nose Projectiles [J]. Mech Mater, 1990, 10(1-2): 97-105.

[14] Warren T L. The Effect of Strain Rate on the Dynamic Expansion of Cylindrical Cavities [J]. J Appl Mech, 1999, 66(3): 818-821.

[15] Zhou H, Wen H M. Dynamic Cylindrical Cavity Expansion Model and Its Application to Penetration Problems [J]. Chinese Journal of High Pressure Physics, 2006, 20(1): 57-78. (in Chinese)
周 辉, 文鹤鸣. 动态柱形空穴膨胀模型及其在侵彻问题中的应用 [J]. 高压物理学报, 2006, 20(1): 57-78.

[16] Warren T L, Hanchak S J, Poormon K L. Penetration of Limestone Targets by Ogive-Nosed VAR 4340 Steel Projectiles at Oblique Angles: Experiments and Simulations [J]. Int J Impact Eng, 2004, 30(10): 1307-1331.

[17] Wen H M. Predicting the Penetration and Perforation of FRP Laminates Struck Normally by Projectiles with Different Nose Shapes [J]. Compos Struct,2000,49(3):321-329.
[18] Wen H M. Penetration and Perforation of Thick FRP Laminates [J]. Compos Sci Technol,2001,61(8):1163-1172.
[19] Chen X W,Li Q M. Perforation of a Thick Plate by Rigid Projectiles [J]. Int J Impact Eng,2003,28(7):743-759.
[20] He T,Wen H M,Qin Y. Finite Element Analysis to Predict Penetration and Perforation of Thick FRP Laminates Struck by Projectiles [J]. Int J Impact Eng,2008,35(1):27-36.
[21] He T,Wen H M,Qin Y. Penetration and Perforation of FRP Laminates Struck Transversely by Conical-Nosed Projectiles [J]. Compos Struct,2007,81(2):243-252.
[22] Ben-Dor G,Dubinsky A,Elperin T. Ballistic Impact:Recent Advances in Analytical Modeling of Plate Penetration Dynamics—A Review [J]. Appl Mech Rev,2005,58(6):355-371.
[23] He T. A Study on the Penetration of Projectiles into Targets Made of Various Materials [D]. Hefei:University of Science and Technology of China,2007. (in Chinese)
何　涛. 动能弹在不同材料靶体中的侵彻行为研究 [D]. 合肥:中国科学技术大学,2007.
[24] Wen H M,Jones N. Low-Velocity Perforation of Punch-Impact-Loaded Metal Plates [J]. J Pressure Vessel Technol,1996,118(2):181-187.
[25] Woodward R L. The Penetration of Metal Targets by Conical Projectiles [J]. Int J Mech Sci,1978,20(6):349-359.
[26] Radin J,Goldsmith W. Normal Projectile Penetration and Perforation of Layered Targets [J]. Int J Impact Eng,1988,7(2):229-259.
[27] Rosenberg Z,Forrestal M J. Perforation of Aluminum Plates with Conical-Nosed Rods—Additional Data and Discussion [J]. J Appl Mech,1988,55(1):236-238.

锥头弹丸撞击下固支金属厚靶的侵彻与穿透的理论研究

孙炜海,文鹤鸣

(中国科学技术大学中国科学院材料力学行为和设计重点实验室,安徽合肥　230027)

摘要:研究了在不同速度的刚性锥头弹丸撞击下固支金属厚靶的侵彻和穿透性能。假定靶板的变形是局部化的,且冲击能量仅通过侵彻过程吸收,同时假定弹体在侵彻过程中表面所受靶体的平均压力是由基于空穴膨胀理论的靶体材料弹塑性变形所引起的静态阻力以及速度效应引起的动阻力两部分组成,认为侵彻过程中靶体对弹体的静阻力要进行自由表面效应修正,而且动阻力是瞬时侵彻速度的函数。获得了锥头弹丸在侵彻和贯穿过程中的弹道极限速度和残余速度的公式。将理论预测与实验结果进行比较,发现两者符合得很好。

关键词:锥头弹丸;金属厚靶板;弹道极限;穿透;残余速度

中图分类号:O385　　**文献标识码**:A